Influence of Severe Plastic Deformation on the Magnetic Properties of Sm-Co Permanent Magnets

*Alexander Paulischin, Lukas Weissitsch, Stefan Wurster, Simon Fellner, Heinz Krenn, Andrea Bachmaier**

Alexander Paulischin, Lukas Weissitsch, Stefan Wurster, Simon Fellner, Andrea Bachmaier
Erich Schmid Institute of Materials Science of the Austrian Academy of Sciences
Jahnstrasse 12
8700 Leoben, Austria
E-mail: andrea.bachmaier@oeaw.ac.at

Heinz Krenn
Institute of Physics
Universitätsplatz 5
8010 Graz, Austria

Keywords: Severe Plastic Deformation, High Pressure Torsion, Hard Magnetic Materials, Nanostructured Materials, Nanocrystalline Magnets, Sm-Co Magnets

High pressure torsion (HPT) is presented as a new fabrication route to produce bulk Sm-Co magnets with a strongly refined microstructure down to the nanometer regime. The initial powders, based on the compositions $SmCo_5$, Sm_2Co_7 and Sm_2Co_{17}, are compacted and subsequently deformed by HPT. The microstructural evolution in dependence on the applied deformation parameters is characterized by electron microscopy and the effect of HPT on the phase stability is monitored by synchrotron X-ray diffraction. An increasing amount of applied strain leads to a stronger reduction in grain size while strain localization counteracts a homogeneous microstructural refinement. The positive effect of elevated deformation temperatures is demonstrated for Sm_2Co_{17}, which promotes homogeneous grain refinement, but causes strain induced phase transformations at the same time, strongly affecting the magnetic behavior. SQUID magnetometry is used to characterize the magnetic properties after HPT-

deformation, which indicates the formation of a magnetic texture depending on the respective phase.

1. Introduction

State of the art rare-earth permanent magnets (REPMs) based on the binary combination of Sm and Co are of great interest for today´s society due to their high saturation magnetization M_s and anisotropy field H_a. Especially their high Curie temperature T_c and thus their applicability and magnetic stability at elevated temperatures, as well as their better corrosion resistance makes them suitable candidates for applications far beyond the temperature limit of NdFeB-REPMs. Multiphase magnets based on the Sm_2Co_{17}-phase can perform at temperatures up to 550 °C, making Sm-Co magnets a suitable candidate for e.g. future automotive applications.[1] The conventional fabrication route of these Sm-Co REPMs is based on powder metallurgical processes, containing production steps like milling, powder compaction, sintering and subsequent heat treatments. A drawback of this fabrication route is the necessity of a complex, multistep heat treatment to achieve suitable magnetic properties, which makes it energy-, time- and thus cost-consuming.[1][2]

Over the last decades, ongoing research has been focused on the improvement of magnetic properties by nanocrystalline microstructures and hard/soft magnetic nanocomposites. Grain refinement down to the single domain size is used to tailor the magnetic properties, as it is accompanied by an increase in coercivity H_c. In addition, grain size reduction facilitates exchange coupling between soft and hard magnetic phases, leading to an increasing energy product by a simultaneous reduction of the hard magnetic phase content and hence material cost.[1][3]–[5]

In contrast to the Co-rich Sm_2Co_{17}- and $SmCo_5$-phase, Sm-rich phases like Sm_2Co_7 are of no commercial interest by now, due to their comparable low M_s and T_c. Yet, the already reported strong increase in H_c, achieved by a grain size reduction, makes Sm-rich phases like Sm_2Co_7 or $SmCo_3$ potential hard magnetic phases in nanocomposite magnets.[1][6]–[10]

Thus, new fabrication methods for the production of nanostructured Sm-Co magnets emerged. Nanocrystalline or even amorphous precursors can be obtained by rapid quenching, high energy ball milling (HEBM), hydrogen assisted processing or a combination of these methods. Fabrication of bulk, nanocrystalline magnets with isotropic magnetic properties is achieved by spark plasma sintering (SPS) or hot compaction of the precursors. A tuning of the magnetic anisotropy is obtained by hot deformation, further improving magnetic properties.[11]–[21]

A novel approach to fabricate nanostructured REPMs is by the application of severe plastic deformation (SPD). Exceptional grain refinement down to the nanometer regime is achieved, resulting in enhanced mechanical and functional properties.[22][23] Using high pressure torsion

(HPT) deformation, a method of SPD, high torsional strain under hydrostatic pressure is applied, resulting in bulk, disc-shaped samples. Strong microstructural refinement, texture formation as well as phase transformations are some advantages of this fabrication method. Due to the free selection of starting materials – either bulk materials or powders – a broad variety of material combinations can be processed.[22][24]–[27] These advantages make HPT-deformation an interesting processing route for the production of bulk, nanostructured magnets and magnetic nanocomposites with anisotropic magnetic properties.[28]–[35]

In this study, we present a novel approach to process Sm-Co permanent magnets by HPT. This fabrication process combines powder compaction and grain refinement in a single processing step. Depending on the respective deformation parameters, the fabricated Sm-Co magnets have a strongly refined microstructure down to the nanometer range, affecting the magnetic properties. Besides the strong grain refinement, texture formation by HPT-processing further tailors the magnetic behavior. In addition, the applied severe deformation offers the opportunity to achieve strain induced phase transformation, which shows a strong impact on the magnetic properties.

2. Results

2.1. HPT-deformation at room temperature

2.1.1. $SmCo_5$

The microstructural evolution of $SmCo_5$ after compaction and applying a different number of rotations is illustrated in **Figure 1** (a)-(c). The original powder particles are visible in the compacted sample, which have been mainly deformed by compression (**Figure 1** (a)). The differences in contrast in the back scattered electron (BSE) images arises from an inhomogeneous distribution of Sm and Co. Brighter microstructural features contain more Sm, which was confirmed by energy dispersive X-ray spectroscopy (EDX) measurements (not shown). In the $SmCo_5$ sample deformed for 10 rotations at room temperature (RT), a strong refinement of the microstructure is observed (**Figure 1** (b)). Due to the applied torsional deformation, the grains are sheared against each other, resulting in a grain size reduction in axial direction and an increased aspect ratio in radial direction. The microstructural refinement is, however, heterogeneous and areas, in which plastic deformation is localized in shear bands, are highlighted within red dotted lines. As the number of rotations is increased to 20, a homogenization of the microstructural refinement is observed (**Figure 1** (c)). Strain localization becomes less pronounced. Still, radially oriented areas which experienced less deformation than the surrounding microstructure are present. A decreasing BSE contrast with increasing number of rotations is visible in **Figure 1** (a)-(c), indicating that chemical inhomogeneities are averaged by (SPD).

In **Figure 1** (d) the corresponding synchrotron wide angle X-ray scattering (WAXS) patterns measured at a radial position of 3 mm are shown. Although deviations in the chemical distribution of Sm are detected in the as-compacted state by EDX, all peaks of the determined diffraction patterns are attributed to $SmCo_5$ ($CaCu_5$-type). Strain induced phase transformation by HPT-deformation is not observed. A strong peak broadening appears after deformation with 10 and 20 rotations, confirming the observed microstructural refinement.

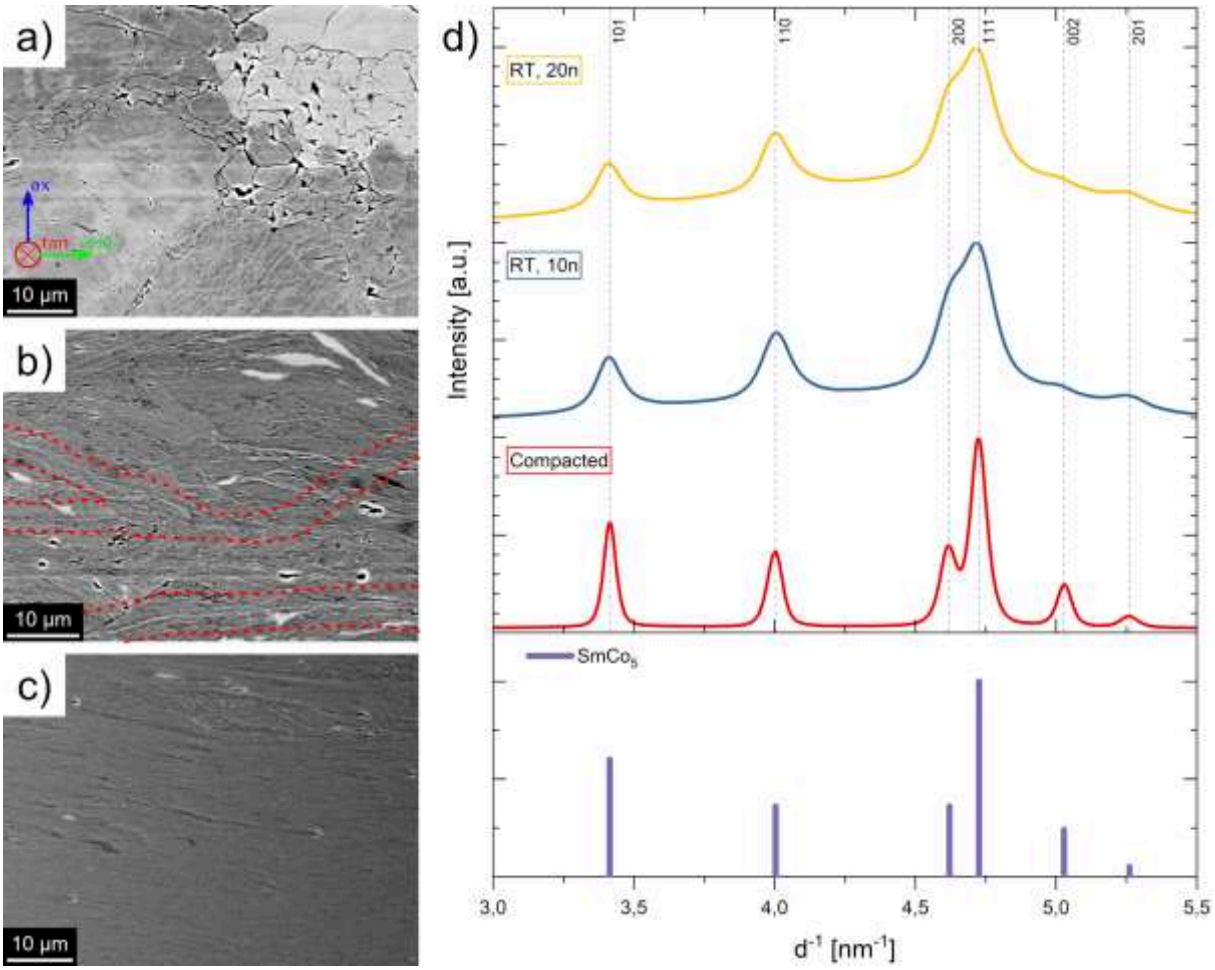

Figure 1. BSE images of $SmCo_5$-samples at a radial position of 3 mm after (a) compaction as well as after HPT-deformation at RT with (b) 10 and (c) 20 rotations. Some areas, where shear bands are present, are highlighted inside red dotted lines. The coordinate system in (a) refers to all subsequent BSE images. The corresponding WAXS diffraction patterns are shown in (d). The positions and intensities of the reference patterns are illustrated as colored bars in the lower section.

A further increase in the number of rotations from 10 to 20 does not lead to stronger peak broadening, but an increase in the background signal is observable. With increasing applied deformation, the intensity ratio of the (200)-peak in relation to the (111)-peak rises, while the relative intensities of the (002)- and the (101)-peaks decrease compared to the (111)-peak, indicating the formation of a texture.

Magnetic properties are measured for all $SmCo_5$ samples (**Figure 2**) and summarized in **Table 1**. **Figure 2** (a) illustrates the magnetic hysteresis loops measured with the applied magnetic field in radial direction in dependence on the number of rotations. HPT-deformation for 10 rotations leads to an increase of H_c to 5.92 kOe compared to the compacted state (3.65 kOe).

However, no improvement in remanence M_r and saturation magnetization M_s is observed. In contrast, further HPT-deformation up to 20 rotations does not significantly improve H_c, but leads to an increasing M_r and M_s. To study the influence of HPT-deformation on magnetic anisotropy, magnetic properties of the sample deformed for 20 rotations were measured in radial, tangential and axial direction (**Figure 2** (b)). Magnetic properties in tangential direction show similar characteristics as in radial direction. Only slight differences in H_c, M_r and M_s are present. In contrast, the measurement in the axial direction shows a pronounced increase of H_c, M_r and with M_s being comparable in the tangential direction.

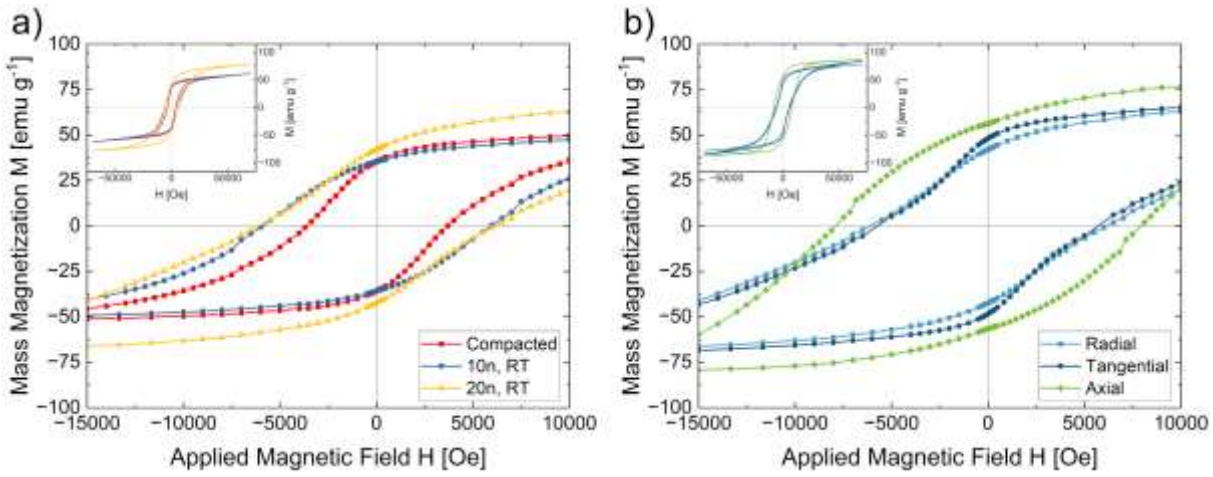

Figure 2. Hysteresis loops of $SmCo_5$-specimens measured with the applied magnetic field in (a) radial direction after HPT-deformation with different deformation parameters and (b) radial, tangential and axial direction after HPT-deformation with 20 rotations at RT.

Table 1. Coercivity H_c, remanence M_r and saturation magnetization M_s of $SmCo_5$ for different number of rotations and applied magnetic field directions.

Deformation parameter	Measurement direction	H_c [kOe]	M_r [emu g^{-1}]	M_s [emu g^{-1}]
Compacted	Radial	3.65	35.60	71.97
10n, RT	Radial	5.92	35.55	73.48
20n, RT	Radial	6.12	42.14	87.44
	Tangential	5.70	48.24	94.43
	Axial	7.91	56.40	93.81

2.1.2. Sm_2Co_7

A similar deformation behavior and microstructural evolution is observed for HPT deformed Sm_2Co_7 samples (**Figure 3** (a)-(d)). The strong contrast visible in the compacted sample again arises from chemical inhomogeneities (**Figure 3** (a)), where darker grains contain a higher Co-concentration. The applied shear deformation, as for $SmCo_5$, leads to microstructural refinement and an averaging of the chemical inhomogeneities, as it can be seen by diminishing contrast in **Figure 3** (b)-(d). However, similar microstructures are observed for 10, 20 and 50 rotations and a homogeneous microstructure is not achieved. Even after 50 revolutions, microstructural features with sizes of several micrometers are still present (**Figure 3** (d)). In addition, cracks are observed.

Figure 3 (e) illustrates synchrotron WAXS patterns corresponding to the above-described microstructures. In the compacted state, the Sm_2Co_7-phase is present. In addition, some peaks can be attributed to the $SmCo_5$-phase. Some minor peaks of d^{-1} values between 3.5 nm^{-1} and 4 nm^{-1} cannot be matched with those or other Sm-Co phases. The strong peak broadening after deformation with 10 rotations again confirms the observed initial microstructural refinement by applying SPD. No further peak broadening can be seen for higher numbers of rotations, which is in agreement with the observed microstructural states.

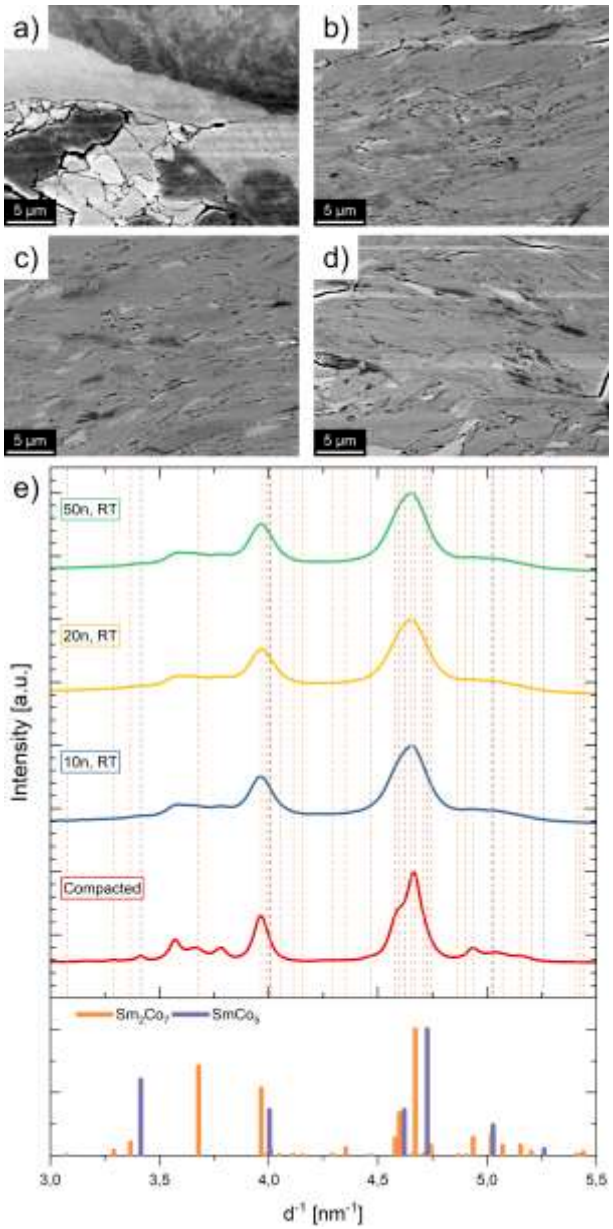

Figure 3. BSE images of Sm_2Co_7-samples at a radial position of 3 mm after (a) compaction as well as HPT-deformation at RT with (b) 10, (c) 20 and (d) 50 rotations. The corresponding WAXS pattern are shown in (e). The positions and intensities of the reference patterns are illustrated as colored bars in the lower section.

Magnetic hysteresis loops of the Sm_2Co_7 samples are shown in **Figure 4** and summarized in **Table 2**. H_c rapidly increases from 2.96 kOe in the compacted state to 8.29 kOe for the sample deformed with 10 rotations (**Figure 4** (a)). In contrast, M_r and M_s show a minor increase by the applied deformation. After 20 rotations, H_c increases to 10.42 kOe. A further increase to 50 rotations does not lead to further enhancement of H_c.

To study the influence of HPT-deformation on magnetic anisotropy, magnetic hysteresis loops of the sample deformed for 50 rotations were measured in radial, tangential and axial direction

(**Figure 4** (b)). In contrast to the $SmCo_5$ sample, magnetic measurements in radial direction exhibits the highest H_c. While the coercivity gradually decreases from radial to axial direction, a strong enhancement of M_r is achieved in axial direction compared to the radial-tangential plane.

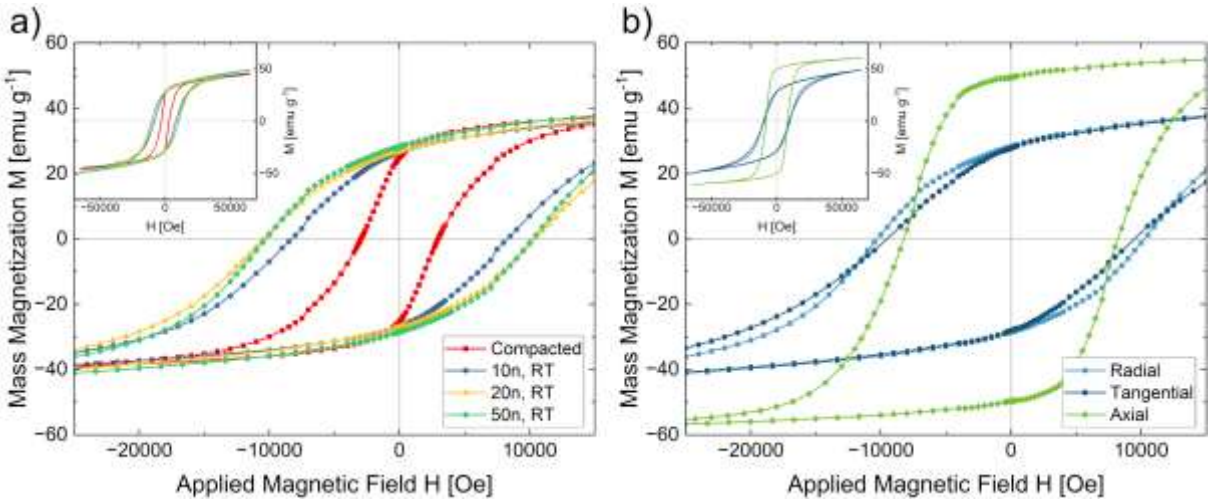

Figure 4. Hysteresis loops of Sm_2Co_7-specimens measured with the applied magnetic field in (a) radial direction after HPT-deformation with different numbers of rotations and (b) radial, tangential and axial direction for the sample deformed for 50 rotations at RT.

Table 2. Coercivity H_c, remanence M_r and saturation magnetization M_s of Sm_2Co_7 for different number of rotations and applied magnetic field directions.

Deformation parameter	Measurement direction	H_c [kOe]	M_r [emu g^{-1}]	M_s [emu g^{-1}]
Compacted	Radial	2,96	25.09	51.83
10n, RT	Radial	8.29	26.62	55.66
20n, RT	Radial	10.42	26.92	59.09
50n, RT	Radial	10.27	28.36	58.45
	Tangential	9.48	27.90	58.44
	Axial	8.23	49.56	64.63

2.1.3. Sm_2Co_{17}

In contrast to the investigated binary $SmCo_5$- and Sm_2Co_7-phase, the investigated Sm_2Co_{17}-phase is based on a commercially available alloy and contains Fe, Cu and Zr besides Sm and Co. The chemical composition of the starting powder, determined by EDX, consists of 51.6 wt.% Co, 25.4 wt.% Sm, 15.4 wt.% Fe, 5.0 wt.% Cu, and 2.6 wt.% Zr.

The microstructure after HPT deformation is illustrated in **Figure 5**. In the compacted state, a coarse-grained structure is visible (**Figure 5** (a)). After 10 rotations, deformed grains appearing shortened in axial direction are visible (**Figure 5** (b)), resulting in an increased aspect ratio in radial direction. A higher amount of deformation causes a strong microstructural refinement. However, the microstructures after 20 rotations (**Figure 5** (c)) and 50 rotations (**Figure 5** (d)) show heterogeneous, lamellar structures with grains in the size of several micrometers surrounded by strongly deformed areas containing nanostructured features. In addition, shear band formation can be observed (inside red dotted lines).

The corresponding WAXS diffraction patterns are illustrated in **Figure 5** (e). Peak broadening is observed after SPD at RT due to microstructural refinement. In addition, no phase transformations due to SPD at RT are present and the same peaks as in the compacted sample state are observed.

The determination of the present phases in the Sm_2Co_{17} samples is not a straightforward task due to the presence of Fe, Cu and Zr as alloying elements. In the compacted state, the positions and sequence of the reference peak intensities of the hexagonal Th_2Ni_{17}-type Sm_2Co_{17}-patterns fit the measured diffraction patterns quite well although all peak positions of the reference patterns are shifted to higher d^{-1}-values. These peak shifts may be caused by lattice straining due to the inclusion of alloying elements in the Sm_2Co_{17}-cells or due to stresses induced by plastic deformation. Although the hexagonal lattice structure belongs to the high temperature modification of the Sm_2Co_{17}-phase, the pattern fits better to the measured spectra than the rhombohedral Th_2Zn_{17}-type RT modification. The stability of the hexagonal modification at RT in nanocrystalline Sm_2Co_{17} has been confirmed.[18] Besides both Sm_2Co_{17} modifications, the metastable, hexagonal $SmCo_7$-phase ($TbCu_7$-type) possesses stability at RT.[18] The reference peaks of $SmCo_7$ fit to most peaks of the measured diffraction patterns, although their intensities show some deviations. The reference diffraction pattern of $SmCo_7$ was constructed using the cell parameters given in reference [6]. In addition, the diffraction pattern of $SmCo_5$ and its sequence of peak intensities shows acceptable accordance with the measured spectra.

To summarize, the compacted sample is assumed to mainly consist of the hexagonal Sm_2Co_{17}-, the $SmCo_7$- and the $SmCo_5$-phase. However, the presence of further phases in small amounts cannot be excluded. After SPD, peak broadening complicates a decisive phase determination. However, it is assumed that the same phases are present after RT deformation.

Magnetic hysteresis loops of the Sm_2Co_{17} samples are shown in **Figure 5** (f) and summarized in **Table 3**. Compared to the compacted state, even a low amount of deformation (10 rotations) shows a significant improvement of H_c. After 20 rotations, slightly higher values of M_r and M_s are obtained. Surprisingly, the magnetic properties of the sample deformed for 50 rotations is similar to the sample deformed for 10 rotations. It is assumed that the reason can be found in the observed stronger strain localization, which causes the formation of a higher number of shear bands leading to less global microstructural refinement in this sample (**Figure 5** (c) and (d)).

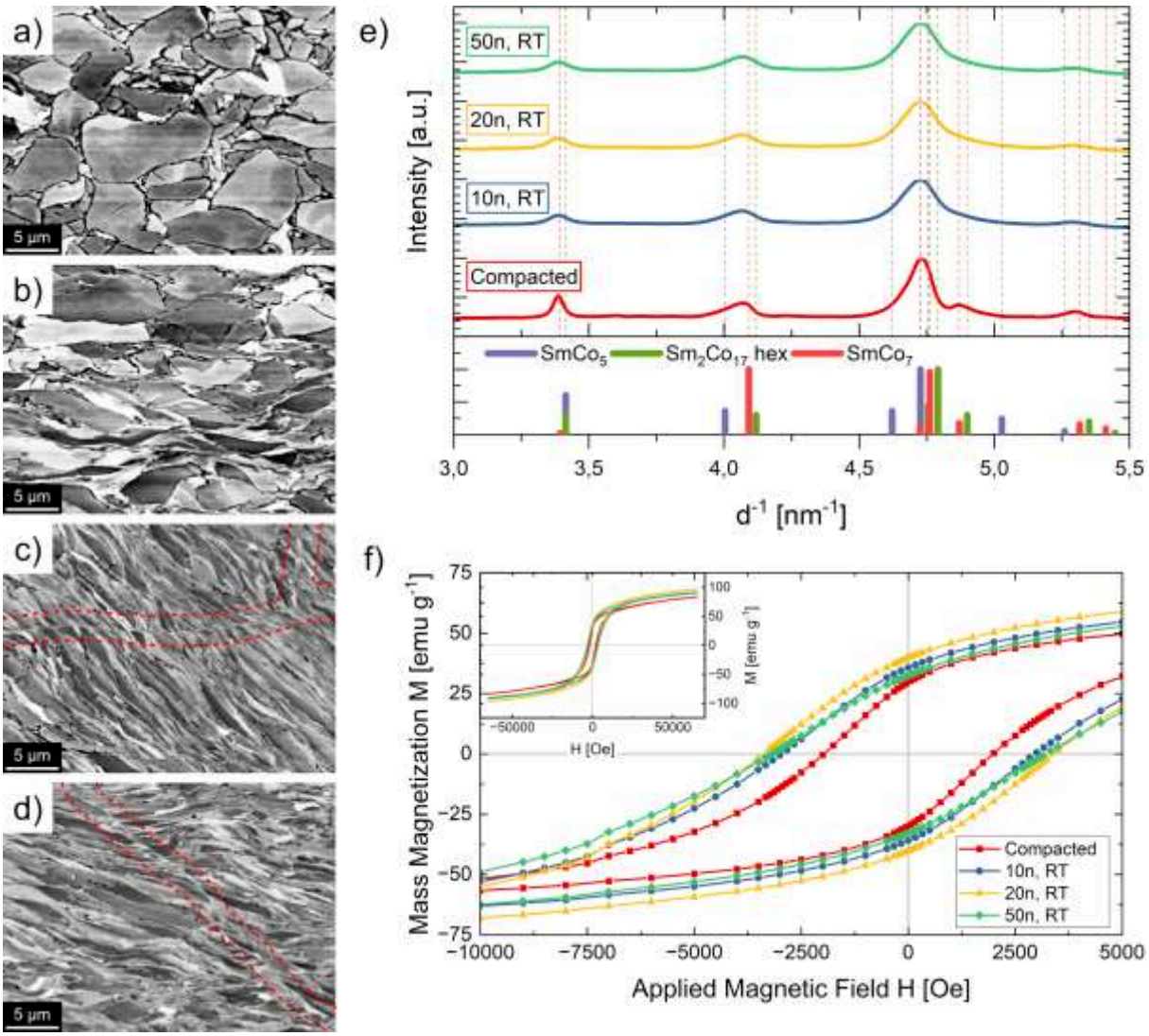

Figure 5. BSE images of Sm_2Co_{17}-specimens at a radial position of 3 mm after (a) compaction as well as HPT-deformation at RT with (b) 10, (c) 20 and (d) 50 rotations. Some areas, in which shear bands are present, are highlighted inside red dotted lines. The corresponding WAXS diffraction patterns are shown in (e). The positions and intensities of the reference patterns are illustrated as colored bars in the lower section. (f) Hysteresis loops of Sm_2Co_{17}-specimens measured with the applied magnetic field in radial direction after HPT-deformation with different rotations at RT.

Table 3. Coercivity H_c, remanence M_r and saturation magnetization M_s of Sm_2Co_{17} for different number of rotations and applied magnetic field directions.

Deformation parameter	Measurement direction	H_c [kOe]	M_r [emu g^{-1}]	M_s [emu g^{-1}]
Compacted	Radial	1.98	29.72	100.72
10n, RT	Radial	2.96	35.80	104.05
20n, RT	Radial	3.39	39.99	110.36
50n, RT	Radial	3.20	32.67	105.90
50n, 250 °C	Radial	1.13	39.66	110.38
	Tangential	0.99	26.13	106.41
	Axial	1.50	22.49	109.74
50n, 400 °C	Radial	3.73	39.03	109.16
	Tangential	3.78	47.80	114.40
	Axial	3.99	51.84	106.73

2.2. HPT-deformation at elevated temperature

To reduce strain localization and promote homogeneous microstructural refinement, HPT-deformation of Sm_2Co_{17} samples were additionally deformed with 50 rotations at elevated deformation temperatures of 250 °C as well as 400 °C. BSE images of the microstructures after HPT-deformation at 250 °C and 400 °C are shown in **Figure 6** (a) and (b), respectively. SPD at 250 °C hinders strain localization and promotes the formation of a homogeneous microstructure. Compared to the microstructure after deformation at RT, no contrast variations are visible after deformation at 250 °C, indicating microstructural refinement down to the nanometer regime. After HPT-deformation at 400 °C, microstructural features like shear bands and grain structures can be observed. As a drawback, the strong microstructural refinement is accompanied by the formation of a fine crack network, which deteriorates mechanical stability.

To get a detailed view on the microstructural evolution after HPT-deformation at 250 °C (**Figure 6** (a)), bright-field scanning transmission electron microscopy (BF-STEM) images were conducted (**Figure 6** (c)). A microstructure with equiaxed grains and a homogeneous grain size distribution is formed by SPD. The mean grain size is estimated to be approximately 20 nm.

WAXS measurements show that deformation at elevated temperatures leads to phase transformations **(Figure 6** (d)). The strongest change is observed at a deformation temperature of 250 °C, but also after deformation at 400 °C, a substantial number of new peaks is formed. In addition to Sm-Co phases, the positions and peak intensities of CoFe are in accordance with some peaks of the measured spectra. The formation of CoFe might cause a depletion of Co and Fe in the Sm-Co phases, which is accompanied by the formation of Sm-rich Sm-Co phases like the Sm_2Co_7- or the $SmCo_3$-phase. The orange arrows in **Figure 6** (d) indicate growing peaks corresponding to Sm-rich phases of Sm and Co, strongly supporting the assumption of the formation of CoFe.

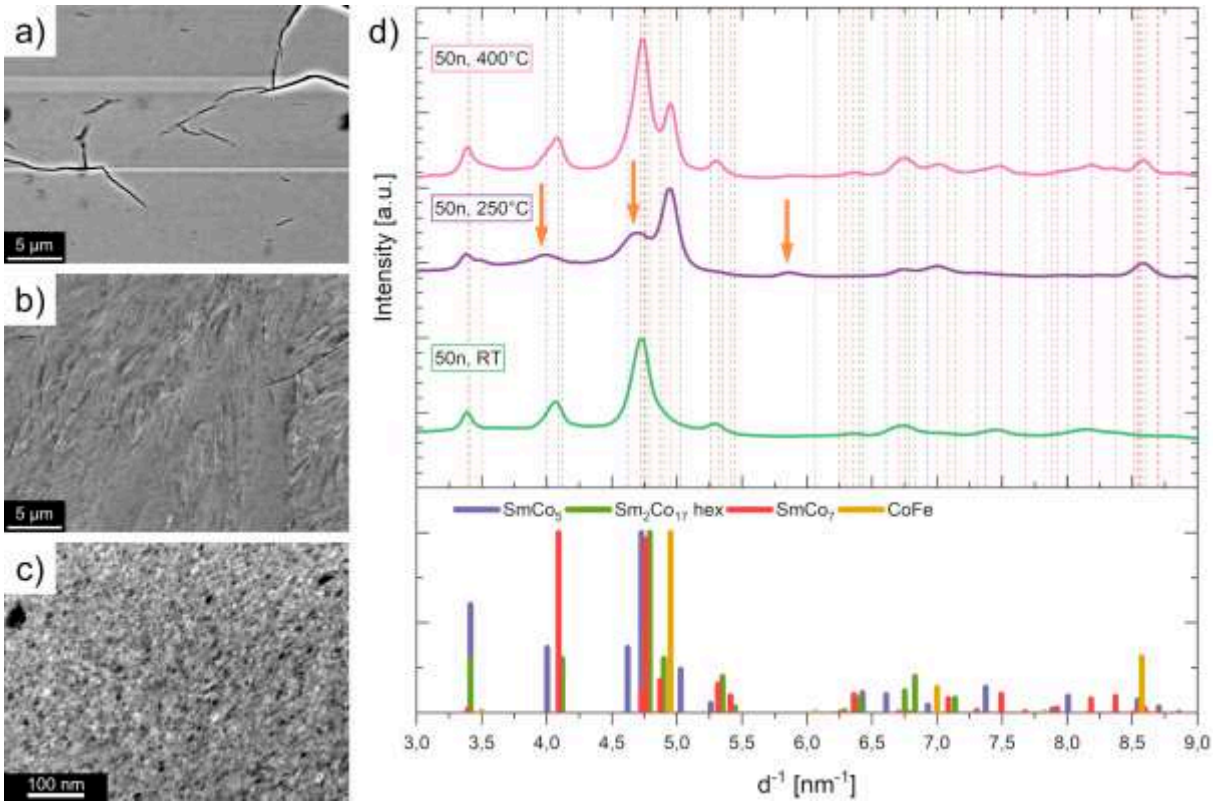

Figure 6. BSE images of Sm_2Co_{17}-specimens at a radial position of 3 mm after HPT-deformation with 50 rotations at (a) 250 °C and (b) 400 °C. (c) BF-STEM image at a radial position of 3 mm after HPT-deformation with 50 rotations at 250 °C. The corresponding WAXS diffraction patterns compared to the diffraction pattern after HPT-deformation at RT with 50

rotations are shown in (d). The positions and intensities of the reference patterns are illustrated as colored bars in the lower section. The orange arrows indicate peaks corresponding to Sm-rich phases.

Figure S1 (a)-(c) illustrates the intensity plots of the WAXS patterns after HPT-deformation with 50 rotations in dependence on the radial position of the HPT disc at RT, 250 °C and 400 °C, respectively. The amount of phase transformation at the deformation temperatures of 250 °C and 400 °C strongly depends on the radial position und thus on the applied torsional strain γ.
Figure 7 (a) displays a comparison of hysteresis loops of Sm_2Co_{17}-samples after compaction as well as after deformation with 50 rotations at RT and elevated temperatures. The compacted, RT and 400 °C deformed sample show similar characteristics in radial direction. After deformation at 400 °C, the highest H_c in radial direction with a value of 3.73 kOe and a remanence of 39.03 emu g^{-1} are achieved. For the sample deformed at 250 °C, the measured hysteresis is significantly different. A sharp drop in H_c down to 1.13 kOe is observed and magnetic saturation is also obtained at lower applied magnetic fields. The magnetic character becomes softer.
To study the influence of HPT-deformation on magnetic anisotropy, measurements in different directions are conducted after deformation at 250 °C and 400 °C (**Figure 7** (b) and (c)). The hysteresis loop in axial direction shows the lowest inclination compared to the radial and tangential direction. Deviations in H_c and M_s are small compared to the strong variation in M_r, especially between radial and axial direction, ranging from 22.49 emu g^{-1} in axial direction to 39.66 emu g^{-1} in radial direction. The opposite is observed for the sample deformed at 400°C (**Figure 7** (c)). M_r ranges from 39.03 emu g^{-1} in radial direction up to 51.84 emu g^{-1} in axial direction. Similar to the sample deformed at 250°C, only slight deviations of H_c as function of measurement direction are present.

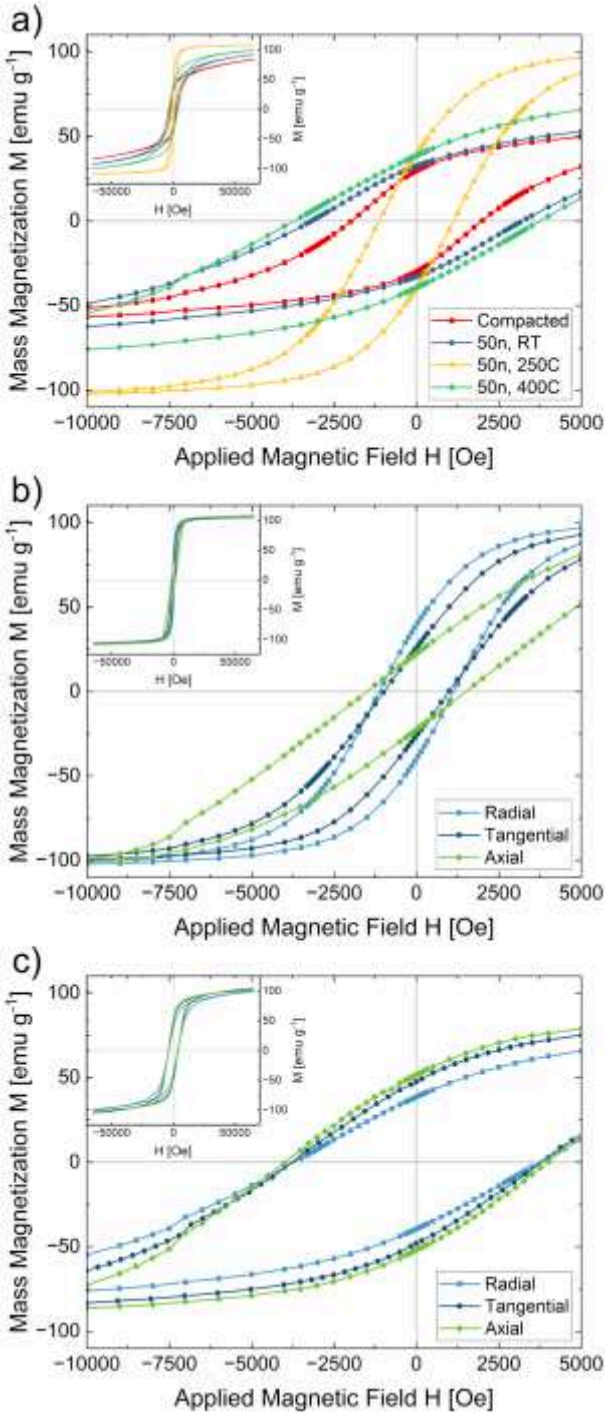

Figure 7. (a) Hysteresis loops of Sm_2Co_{17}-specimens measured with the applied magnetic field in (a) radial direction after HPT-deformation at different temperatures as well as in radial, tangential and axial direction of the samples deformed at (b) 250 °C and (c) 400 °C with 50 rotations.

3. Discussion

SPD processing has a strong influence on the microstructural evolution and the phase stability, strain induced phase formation and consequently on the magnetic properties. In general, an inhomogeneous deformation behavior is observed during SPD of the investigated Sm-Co compounds. Shear localization during HPT-deformation is present for all investigated deformation temperatures leading to heterogeneous microstructural refinement. Strongly deformed and refined areas can be found next to weakly deformed areas with larger microstructural features. The localization of the deformation even leads to the formation of shear bands, where the deformation is localized in narrow deformation paths, while the surrounding microstructure experiences no or little deformation. Second, crack formation is frequently observed and expected to occur upon pressure unloading after HPT-deformation. The cracks strongly vary in length, ranging from several micrometers up to several millimeters. Strain localization and thus an inhomogeneous microstructural refinement as well as the formation of cracks after HPT-deformation were reported for composites consisting of Cu-$SmCo_5$ with low amounts of Cu as well. [29]. In future work, a focus will be placed on further optimization of HPT process parameters.

After HPT processing of pure $SmCo_5$, microstructural refinement without deformation induced phase formations is observed. In general, similar phase stability and microstructural refinement as well as comparable magnetic properties are reported after HPT-deformation of bulk $SmCo_5$ and magnetic composites containing $SmCo_5$ as hard magnetic phase.[29][30][35] Reported values for H_c and M_r of induction-melted $SmCo_5$ ingots after HPT-deformation with 10 rotations are in good agreement with the presented results for HPT-deformed $SmCo_5$ powder. Yet, a lower value for M_s is reported.[35] Higher H_c values reported in Cu-$SmCo_5$ are attributed to the decoupling effect of Cu.[29] However, the Cu addition leads to a decrease in M_r and M_s compared to the results obtained in this study. For the $SmCo_5$-Fe composite, similar M_s and H_c values are reported for samples with an Fe-content of 10 wt.% after HPT-deformation at RT.[30]

The results of the WAXS measurements as well as of the magnetic properties reveal a texture formation due to HPT-deformation, but in different HPT-disc directions. The hysteresis loops in **Figure 2** (b) indicate the formation of a c-axis texture in axial disc direction. This is supported by the results of the WAXS measurements, illustrated in Figure 1 (d), also indicating the alignment of the easy magnetic axis with axial HPT direction. All WAXS measurements are conducted with the synchrotron beam direction parallel to the axial HPT-disc direction. As the number of grains oriented with their (002)-plane perpendicular to the axial disc direction

increases with the number of rotations, the number of grains, whose (002)-plane fulfills the Bragg diffraction condition, declines, resulting in a declining (002)-peak in the measured WAXS-pattern. Thus, a declining (002)-peak is interpreted as an increasing number of grains oriented with their [002]-lattice direction in axial disc direction. This grain orientation due to HPT-deformation leads to the formation of a c-axis texture, which is in agreement with the results of the magnetic measurements. In agreement with the investigated $SmCo_5$ phase, the formation of a pronounced c-axis texture after HPT-processing of $SmCo_5$-Cu composites is reported by Staab et al.[29] In addition to HPT-deformation, the fabrication of nanocrystalline $SmCo_5$ magnets with a pronounced c-axis texture and thus enhanced magnetic properties after HEBM and subsequent hot deformation is reported in several publications.[14][15][36][37] In contrast, wet milling in combination with SPS leads to a comparable magnetic anisotropy but a decrease in H_c.[11]

In Sm_2Co_7, homogeneous microstructures could not be achieved by HPT deformation. No phase formations are observed. An improvement of the magnetic properties of Sm_2Co_7 after processing is obtained similar to other processes (hot plastic deformation or SPS).[8][16] However, a stronger microstructural refinement by HEBM in combination with SPS or hot deformation leads to better magnetic properties. Thus, further improvement of the magnetic properties by SPD might be achieved by optimization of the HPT processing parameters, e.g. by increasing the deformation temperature, to achieve a truly nanocrystalline structure. The observed anisotropic behavior of the magnetic properties after HPT-deformation is in agreement with distinct c-axis textures after hot plastic deformation of Sm_2Co_7.[14][16]

For the investigated Sm_2Co_{17}-compound, HPT deformation at RT leads to similar results in microstructure and magnetic properties, which do not show a strong improvement in comparison to the as-compacted state. Thus, deformation at elevated temperatures was conducted. The variation of the deformation temperature leads to different magnetic characteristics after SPD. Two possible reasons for the observed magnetic softening after deformation at 250 °C are discussed. For spherical particles of the rhombohedral Sm_2Co_{17}-phase, the critical dimension of the single domain size is determined with 3.3 µm while the mean single domain size is about 1.5 µm.[38]. No grain structure is visible in the BSE images after deformation at this temperature indicating a grain size below the resolution of the SEM (c.f. **Figure 6** (a)). An equiaxed grain structure with homogeneous grain size distribution and mean grain size of about 20 nm is determined by STEM investigations (c.f. **Figure 6** (c)), which is far below the reported single domain size of Sm_2Co_{17}. The strong decrease in grain size due to HPT-deformation at 250 °C is an explanation for the observed strong decrease in H_c. No

amorphous microstructure is expected as STEM investigations reveal a nanocrystalline microstructure with homogeneous grain size distribution (c.f. **Figure 6** (c)). Although a microstructural refinement is achieved after HPT-deformation at RT and 400 °C, microstructural features in the size of micrometers are still visible (c.f. **Figure 5** (a)-(d) and **Figure 6** (b)), which fits quite well to the single domain size picture given in literature, explaining the hard magnetic character of the hysteresis loops for theses deformation temperatures.[38]

A second reason for the magnetic softening might be the occurrence of ~~strain induced~~ phase transformation due to HPT-deformation. After deformation at 250 °C, the soft magnetic CoFe phase is detected in the WAXS pattern, which could explain the observed magnetic softening. Despite magnetic saturation is reached at smaller applied fields, an increase in saturation magnetization is not observed. This indicates that the amount of formed CoFe is low and thus pronounced enhancement of M_s is not present. CoFe phase formation is also observed at a deformation temperature of 400 °C. It is assumed that the CoFe amount in this case is even smaller, thus not leading to pronounced magnetic softening.

The formation of CoFe in Sm-Co-Fe-Cu-Zr alloys after arc melting of the initial components is reported by Khudina et al. The CoFe phase remained present during subsequent melt spinning, milling and isothermal aging, while the phase amount showed some variations during the processing steps. Compared to the results obtained in this study, the reported values for H_c are about a magnitude lower while quite comparable values for the saturation magnetization are reported for all fabrication steps. The poor magnetic properties are attributed to the presence of the CoFe phase.[39]

Appearing phase transformations due to SPD can be either strain-induced, pressure-induced or by a combination of pressure and applied strain.[22] In addition, temperature has a strong impact on phase stability and formation. Phase transformation in Sm_2Co_{17} appears only after HPT-deformation at elevated temperatures. (c.f. **Figure 6** (d) and **Figure S1**). Since all samples were deformed with the same nominal pressure, a pressure-induced phase transformation is excluded. As illustrated in **Figure S1**, the intensity of the appearing phase transformation depends on the radial position of the HPT disc and thus is expected to be strain-induced. Still the influence of the deformation temperature on the formation of CoFe cannot be neglected, as the intensity of the CoFe-peak at 250 °C is stronger than at 400 °C, as illustrated in **Figure 6** (d). Deformation at elevated temperatures, especially 250 °C, hinders strain localization and promotes a homogeneous microstructural refinement (c.f. **Figure 6** (a) and (b)). Thus, it is expected, that

the phase formation of CoFe is strain-induced, but the amount of formed CoFe-phase is controlled by the respective deformation temperature.

No formation of a magnetic texture is reported in single- and multiphase alloys containing Sm_2Co_{17}- and metastable $SmCo_7$-phases after HEBM and subsequent hot plastic deformation.[14][15] The observed anisotropic magnetic properties after HPT-deformation at elevated temperatures might thus be attributed to the presence of Sm-rich phases like $SmCo_5$ than to the Sm_2Co_{17}- and $SmCo_7$-phase. In addition, a textured CoFe-phase might lead contribute to the observed anisotropic behavior after deformation at elevated deformation temperatures. The opposing trend of M_r after deformation at 250 °C and 400 °C is mainly attributed to the shape of the respective specimen for magnetic measurements. Yet, it is mentioned, that a correction of the demagnetization factor is not conducted for the provided results.

Ongoing research focusses on a detailed study of the present phases after HPT-deformation and their effect on the magnetic properties and magnetic anisotropy.

4. Conclusion

In the present work, HPT-deformation is successfully used to fabricate bulk Sm-Co magnets from initial powders based on the compositions $SmCo_5$, Sm_2Co_7 and Sm_2Co_{17}. The effect of the applied deformation as well as the deformation temperature on the microstructural refinement, the phase stability and the magnetic properties is studied. The conclusions can be summarized as follows:

- In general, a higher number of rotations leads to a stronger microstructural refinement. For all investigated Sm-Co phases, strong grain refinement, accompanied by an enhanced H_c, is achieved after at least 20 rotations. Thus, HPT is an effective method to tailor magnetic properties.
- Strain localization and the formation of shear bands have a strong influence on the final microstructure and thus the magnetic properties.
- HPT-deformation is an effective way to fabricate bulk Sm-Co magnets with an anisotropic magnetic behavior. The determined magnetic texture of $SmCo_5$ and Sm_2Co_7 is in agreement with reports in literature. In contrast, the formation of a pronounced anisotropic behavior of Sm_2Co_{17} is not been reported yet.[14][15]
- For Sm_2Co_{17}, a homogeneous deformation behavior is promoted at elevated temperatures. Best microstructural refinement is achieved for deformation at 250 °C.
- HPT-deformation at elevated temperatures leads to strain induced phase transformation in Sm_2Co_{17}, which has a strong effect on the magnetic behavior.

5. Experimental

As starting materials, commercial powders of the intermetallic compounds $SmCo_5$ (Alfa Aesar REacton, Sm 33%), Sm_2Co_7 (Sigma-Aldrich) and Sm_2Co_{17} (American Elements 99.9%) were used. To prevent oxidation, the powders were stored and handled in an Ar filled glove box.

The powders were consolidated using an HPT device under a hydrostatic pressure up to 7.5 GPa and a quarter revolution, resulting in dense, bulk samples with a nominal diameter of 8 mm and a height of approximately 1.3 mm. To prevent oxidation during compaction, the powder is sealed in a customized small container filled with Ar, when transported between glove box and HPT-device.[26] In a second step, the compacted samples were HPT deformed under a nominal pressure of 7.5 GPa. Between 10 and 50 rotations were applied with a rotational frequency between 0.6 and 1.2 min^{-1} at deformation temperatures between RT and 400 °C, depending on the respective intermetallic compound. After HPT-deformation, the sample thickness is reduced to ~ 0.7 mm. The HPT setup used in this study is described elsewhere.[40] A summary of the deformation parameters is given in **Table 4**.

During HPT-deformation, the microstructure is sheared in tangential disc direction. The torsional strain γ, applied by HPT-deformation, depends on the number of revolutions n, the radial position r as well as the specimen thickness t, as given by **Equation 1**.[22][23]

$$\gamma = \frac{2\pi n r}{t} \quad (1)$$

To investigate the influence of HPT-deformation on the microstructural and magnetic development, the deformed samples were bisected, as schematically illustrated in **Figure 8**. With respect to the HPT-disc, areas where measurements were conducted are marked. The position of the cut specimen for the superconducting quantum interference device (SQUID) is highlighted in red.

Microstructure investigations were conducted using scanning electron microscopy (SEM; LEO 1525, Carl Zeiss Microscopy GmbH, Oberkochen, Germany) in tangential specimen direction using back scattered electron (BSE) detection mode. Energy dispersive X-ray spectroscopy (EDX XFlash 6-60, Bruker, mounted on SEM TESCAN Magna) with the software package Esprit 2.3 from Bruker was used to determine chemical compositions. On a selected sample, scanning transmission electron microscopy (STEM) investigations were conducted on a JEOL JEM 2200FS TEM working at 200 kV. The scanning of the electron beam was controlled by a TVIPS universal scan generator. As illustrated in **Figure 8**, a cross-sectional lamella for STEM investigations was prepared by focused ion beam (FIB) milling with a lift-out technique using a Zeiss Auriga dual-beam workstation. The lamella was extracted at a radial disc position of 3

mm in the radial-tangential disc plane using an Omniprobe micro-manipulator. Bright-field STEM (BF-STEM) investigations were carried out by viewing the lamella in axial direction of the sample disc.

To investigate crystal structures after HPT-deformation, synchrotron wide angle X-ray scattering (WAXS) measurements in transmission mode were performed in axial disc direction (Petra III: P21.2 synchrotron facility at Deutsches Elektronen-Synchrotron DESY, Hamburg, Germany; beam energy: 82.5 keV; beam size: 200 x 200 μm^2; Petra III: P07b synchrotron facility at DESY, Hamburg, Germany, beam energy: 87.1 keV, beam size: 400 x 10 μm^2). The HPT-discs were screened with a step-size of 0.5 mm or less, as schematically illustrated in **Figure 8**. A LaB_6 reference was used as a calibration source. pyFAI was used to integrate the measured data.[41]

The magnetic properties were determined using a SQUID -magnetometer (Quantum Design MPMS-XL-7, quantum Design, Inc., San Diego, CA, USA) with the operating software MPMSMultiVu application (version 1.54). For the measurements, small box-shaped specimens with an approximate base of 1.5 x 1 mm^2 (radial x tangential) were cut out at a radial position of 3 mm, as depicted in **Figure 8**. The hysteresis measurements were conducted at 300 K in magnetic fields up to 70 kOe. The direction of the magnetic field is applied parallel to the radial HPT-disc direction, except for those specimens, where a SPD induced magnetic anisotropy is determined by measuring all orthogonal directions.

Measurements in tangential and axial direction were conducted on chosen specimens to investigate SPD induced magnetic anisotropy.

For the determination of the saturation magnetization M_s, the mass magnetization M was plotted over the inverse applied magnetic field H^{-1} and the theoretical saturation magnetization was determined by a linear fit for magnetic fields higher than 70 kOe. A correction of the demagnetization factor for magnetic measurements has not been conducted.

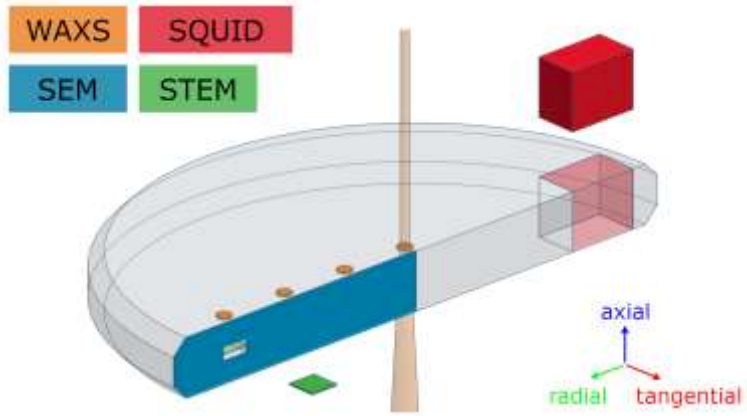

Figure 8. Schematic illustration of a bisected HPT-disc with a nominal diameter of 8 mm. The colored surfaces indicate the areas used for SEM (blue) and WAXS (orange) investigations. The orange beam indicates the WAXS measurement direction. The green FIB lift-out at a radial position of 3 mm is used for STEM investigations. The cut-out, box shaped specimen (red) is used for SQUID magnetometry. The given orthogonal reference system "axial-radial-tangential" is used for all investigations.

Table 4. Summary of HPT deformation parameters for all Sm-Co samples.

Intermetallic compound	Sm-Co	Number of rotations *n*	Deformation temperature [°C]	Rotational frequency [min^{-1}]
$SmCo_5$		10, 20	RT	0.6
Sm_2Co_7		10, 20	RT	0.6
		50		1.2
Sm_2Co_{17}		10, 20	RT	0.6
		50	RT, 250, 400	1.2

[COD 9004229 (CoFe), ICDD 00-026-0484 (Sm_2Co_{17} hexagonal), ICDD 00-027-1122 ($SmCo_5$) and ICSD 98-000-2054 (Sm_2Co_7) contain the supplementary crystallographic data for this paper. The diffraction pattern of $SmCo_7$ was reconstructed using the cell parameters given in reference [6]]

Acknowledgements

This project has received funding from the European Research Council (ERC) under the European Union's Horizon 2020 research and innovation programme, grant agreement No 757333.

We acknowledge DESY (Hamburg, Germany), a member of the Helmholtz Association HGF, for the provision of experimental facilities. Parts of this research were carried out at beamline P21.2 at PETRA III under proposal I-20220454 EC. Parts of this research were carried out at PETRA III and we would like to thank Juraj Todt and Norbert Schell for assistance in using beamline P07b. The authors gratefully acknowledge the financial support from the Austrian Science Fund (FWF): Y1236-N37.

Received: ((will be filled in by the editorial staff))
Revised: ((will be filled in by the editorial staff))
Published online: ((will be filled in by the editorial staff))

References

[1] S. Liu, *Chin. Phys. B* **2019**, *28*, 017501.
[2] J. Cui, J. Ormerod, D. Parker, R. Ott, A. Palasyuk, S. Mccall, M.P. Paranthaman, M.S. Kesler, M.A. McGuire, I.C. Nlebedim, C. Pan, T. Lograsso, *JOM* **2022**, *74*, 1279.
[3] G.C. Hadjipanayis, *J. Magn. Magn. Mater.* **1999**, *200*, 373.
[4] D.C. Jiles, *Acta Mater.* **2003**, *51*, 5907.
[5] O. Gutfleisch, M.A. Willard, E. Brück, C.H. Chen, S.G. Sankar, J.P. Liu, *Adv. Mater.* **2011**, *23*, 821.
[6] X.-Y. Song, Z.-X. Zhang, N.-D. Lu, H.-N. Liang, D.-P. Li, X.-Q. Yan, J.-X. Zhang, *Front. Mater. Sci.* **2012**, *6*, 207.
[7] A. Chrobak, *Materials* **2022**, *15*, 6506.
[8] W. Xu, X. Song, Z. Zhang, H. Liang, *Mater. Sci. Eng. B* **2013**, *178*, 971.
[9] Y. Zhuge, Y. Li, X. Xu, D. Zhang, H. Zhang, W. Liu, M. Yue, *J. Rare Earths* **2021**, *39*, 312.
[10] N. Poudyal, W. Xia, M. Yue, J. Ping Liu, *J. Appl. Phys.* **2014**, *115*, 17A715.
[11] L. Fang, T. Zhang, H. Wang, C. Jiang, J. Liu, *J. Magn. Magn. Mater.* **2018**, *446*, 200.
[12] J. Cui, J. Ormerod, D.S. Parker, R. Ott, A. Palasyuk, S. McCall, M.P. Paranthaman, M.S. Kesler, M.A. McGuire, C. Nlebedim, C. Pan, T. Lograsso, *JOM* **2022**, *74*, 2492.
[13] O. Gutfleisch, A. Bollero, A. Handstein, D. Hinz, A. Kirchner, A. Yan, K.-H. Müller, L. Schultz, *J. Magn. Magn. Mater.* **2002**, *242–245*, 1277.
[14] A.M. Gabay, M. Marinescu, J.F. Liu, G.C. Hadjipanayis, *J. Magn. Magn. Mater.* **2009**, *321*, 3318.
[15] A.M. Gabay, W.F. Li, G.C. Hadjipanayis, *J. Magn. Magn. Mater.* **2011**, *323*, 2470.
[16] Q. Ma, M. Jia, Z. Hu, M. Yue, Y. Liu, T. Zhao, B. Shen, *Chin. Phys. B* **2021**, *30*, 047505.
[17] Z.X. Zhang, X.Y. Song, W.W. Xu, M. Seyring, M. Rettenmayr, *Scr. Mater.* **2010**, *62*, 594.
[18] X. Song, N. Lu, M. Seyring, M. Rettenmayr, W. Xu, Z. Zhang, J. Zhang, *Appl. Phys. Lett.* **2009**, *94*, 023102.
[19] M. Yue, X. Zhang, J.P. Liu, *Nanoscale* **2016**, *8*, 233.
[20] O. Gutfleisch, *J. Phys. Appl. Phys.* **2000**, *33*, R157.

[21] C. Rong, Y. Zhang, N. Poudyal, X. Xiong, M.J. Kramer, J.P. Liu, *Appl. Phys. Lett.* **2010**, *96*, 102513.
[22] K. Edalati, A. Bachmaier, V.A. Beloshenko, Y. Beygelzimer, V.D. Blank, W.J. Botta, K. Bryła, J. Čížek, S. Divinski, N.A. Enikeev, Y. Estrin, G. Faraji, R.B. Figueiredo, M. Fuji, T. Furuta, T. Grosdidier, J. Gubicza, A. Hohenwarter, Z. Horita, J. Huot, Y. Ikoma, M. Janeček, M. Kawasaki, P. Král, S. Kuramoto, T.G. Langdon, D.R. Leiva, V.I. Levitas, A. Mazilkin, M. Mito, H. Miyamoto, T. Nishizaki, R. Pippan, V.V. Popov, E.N. Popova, G. Purcek, O. Renk, Á. Révész, X. Sauvage, V. Sklenicka, W. Skrotzki, B.B. Straumal, S. Suwas, L.S. Toth, N. Tsuji, R.Z. Valiev, G. Wilde, M.J. Zehetbauer, X. Zhu, *Mater. Res. Lett.* **2022**, *10*, 163.
[23] R.Z. Valiev, R.K. Islamgaliev, I.V. Alexandrov, *Prog. Mater. Sci.* **2000**, *45*, 103.
[24] A. Bachmaier, R. Pippan, *Mater. Trans.* **2019**, *60*, 1256.
[25] H. Azzeddine, D. Bradai, T. Baudin, T.G. Langdon, *Prog. Mater. Sci.* **2022**, *125*, 100886.
[26] M. Wurmshuber, S. Doppermann, S. Wurster, D. Kiener, *IOP Conf. Ser. Mater. Sci. Eng.* **2019**, *580*, 012051.
[27] A. Bachmaier, R. Pippan*, *Int. Mater. Rev.* **2013**, *58*, 41.
[28] L. Weissitsch, F. Staab, K. Durst, A. Bachmaier, *Mater. Trans.* **2023**, *64*, 1537.
[29] F. Staab, E. Bruder, L. Schäfer, K. Skokov, D. Koch, B. Zingsem, E. Adabifiroozjaei, L. Molina-Luna, O. Gutfleisch, K. Durst, *Acta Mater.* **2023**, *246*, 118709.
[30] L. Weissitsch, M. Stückler, S. Wurster, P. Knoll, H. Krenn, R. Pippan, A. Bachmaier, *Crystals* **2020**, *10*, 1026.
[31] L. Weissitsch, S. Wurster, M. Stückler, T. Müller, H. Krenn, R. Pippan, A. Bachmaier, *J. Magn. Magn. Mater.* **2023**, *584*, 171082.
[32] H. Li, L. Lou, F. Hou, D. Guo, W. Li, X. Li, D.V. Gunderov, K. Sato, X. Zhang, *Appl. Phys. Lett.* **2013**, *103*, 142406.
[33] A. Hosokawa, K. Takagi, T. Kuriiwa, Y. Inoue, K. Ozaki, *J. Magn. Magn. Mater.* **2019**, *473*, 51.
[34] M. Stückler, L. Weissitsch, S. Wurster, P. Felfer, H. Krenn, R. Pippan, A. Bachmaier, *AIP Adv.* **2020**, *10*, 015210.
[35] F.-Y. Wang, T.-T. Qi, Q. Wu, H. Ge, P.-Z. Si, *AIP Adv.* **2024**, *14*, 015243.
[36] X. Xu, Y. Li, Z. Ma, M. Yue, D. Zhang, *Scr. Mater.* **2020**, *178*, 34.
[37] X. Xu, Y. Li, Y. Teng, T. Wang, H. Zhang, D. Zhang, M. Yue, *Mater. Charact.* **2021**, *173*, 110942.
[38] T. Inoue, K. Goto, *IEEE Transl. J. Magn. Jpn.* **1985**, *1*, 992.
[39] E.V. Khudina, M.V. Zheleznyi, I.O. Minkova, P.S. Rybin, V.P. Menushenkov, *J. Phys. Conf. Ser.* **2019**, *1389*, 012119.
[40] A. Hohenwarter, A. Bachmaier, B. Gludovatz, S. Scheriau, R. Pippan, *Int. J. Mater. Res.* **2009**, *100*, 1653.
[41] G. Ashiotis, A. Deschildre, Z. Nawaz, J.P. Wright, D. Karkoulis, F.E. Picca, J. Kieffer, *J. Appl. Crystallogr.* **2015**, *48*, 510.

Table of Contents

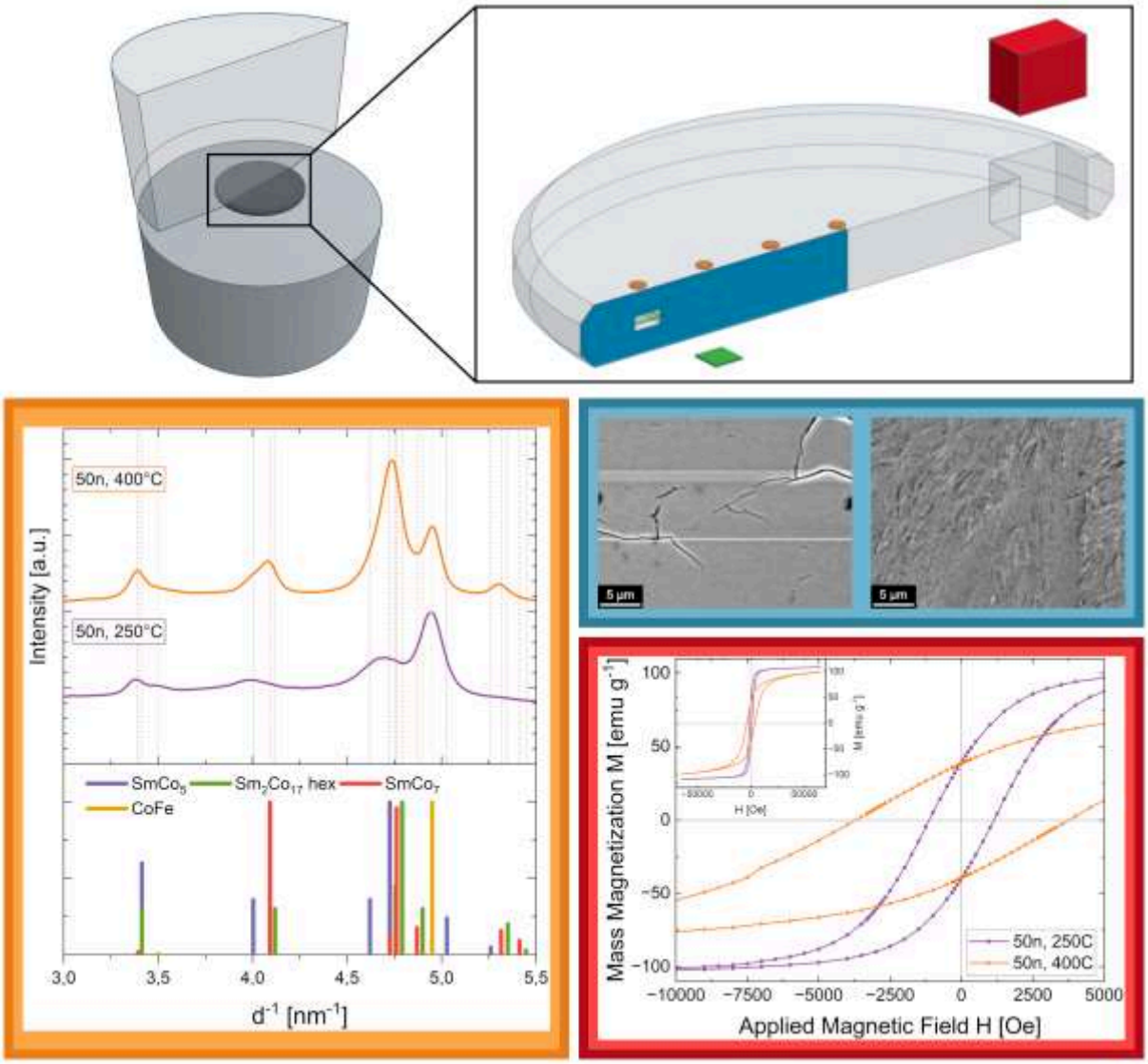

In this study, the influence of severe plastic deformation on the microstructural evolution and magnetic properties of Sm-Co based permanent magnets is investigated. Powders of binary Sm-Co phases 1:5, 2:7 and 2:17 (Sm:Co) are deformed using high pressure torsion. Grain refinement and strain induced phase transformations strongly affect magnetic properties.

Supporting Information

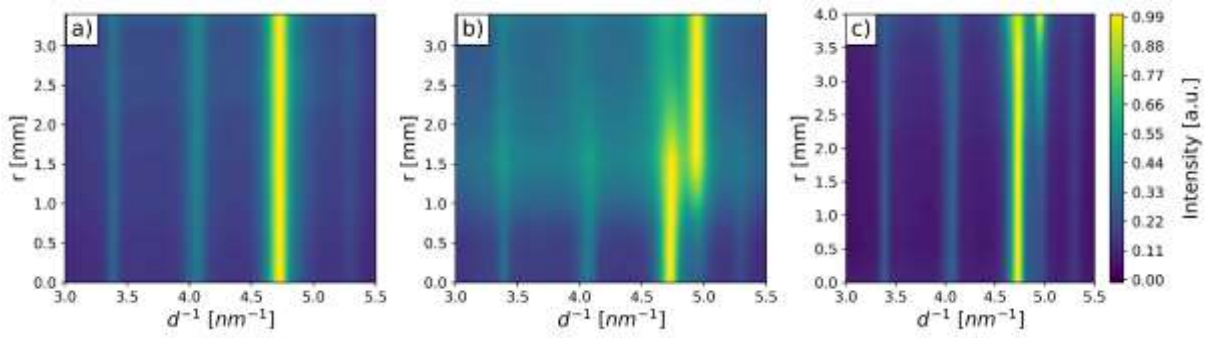

Figure S1. Intensity plots of WAXS patterns of Sm_2Co_{17} after HPT-deformation for 50 rotations at (a) RT, (b) 250°C and (c) 400°C in dependence on the HPT disc radius. The intensity scale bar for all plots is illustrated on the right side.